Research Paper

An autopsy study of the spectrum of severe COVID-19 in children: From SARS to different phenotypes of MIS-C

Amaro Nunes Duarte-Neto[a,b,1], Elia Garcia Caldini[a,1], Michele Soares Gomes-Gouvêa[c], Cristina Takami Kanamura[b], Renata Aparecida de Almeida Monteiro[a], Juliana Ferreira Ferranti[d], Andrea Maria Cordeiro Ventura[e], Fabiane Aliotti Regalio[f], Daniela Matos Fiorenzano[d], Maria Augusta Bento Cicaroni Gibelli[d], Werther Brunow de Carvalho[d], Gabriela Nunes Leal[d], João Renato Rebello Pinho[c], Artur Figueiredo Delgado[d], Magda Carneiro-Sampaio[d], Thais Mauad[a], Luiz Fernando Ferraz da Silva[a,g], Paulo Hilario Nascimento Saldiva[a], Marisa Dolhnikoff[a,*]

[a] Departamento de Patologia, Faculdade de Medicina da Universidade de São Paulo. Av. Dr. Arnaldo, 455, 01246-903 São Paulo, SP, Brasil
[b] Instituto Adolfo Lutz. Av. Dr. Arnaldo, 351, 01246-000 São Paulo, SP, Brasil
[c] Departamento de Gastroenterologia, LIM 07, Faculdade de Medicina da Universidade de São Paulo. Av Dr Enéas de Carvalho Aguiar, 500, 05403-000 São Paulo, SP, Brasil
[d] Instituto da Criança, Departamento de Pediatria, Faculdade de Medicina da Universidade de São Paulo. Av Dr Enéas de Carvalho Aguiar, 647, 05403-000 São Paulo, SP, Brasil
[e] Unidade de Terapia Intensiva Pediátrica, Departamento de Pediatria, Hospital Universitário da Universidade de São Paulo. Av. Prof. Lineu Prestes, 2565, 05508-000 São Paulo, SP, Brasil
[f] Divisão de Anestesia, Hospital das Clínicas da Faculdade de Medicina da Universidade de São Paulo. Av. Dr Enéas de Carvalho Aguiar, 255, 01246-000 São Paulo, SP, Brasil
[g] Serviço de Verificação de Óbitos da Capital, Universidade de São Paulo. Av Dr Enéas de Carvalho Aguiar, 250, 05403-000 São Paulo, SP, Brasil

ARTICLE INFO

ABSTRACT

Background: COVID-19 in children is usually mild or asymptomatic, but severe and fatal paediatric cases have been described. The pathology of COVID-19 in children is not known; the proposed pathogenesis for severe cases includes immune-mediated mechanisms or the direct effect of SARS-CoV-2 on tissues. We describe the autopsy findings in five cases of paediatric COVID-19 and provide mechanistic insight into the mechanisms involved in the pathogenesis of the disease.

Methods: Children and adolescents who died with COVID-19 between March 18 and August 15, 2020 were autopsied with a minimally invasive method. Tissue samples from all vital organs were analysed by histology, electron microscopy (EM), reverse-transcription polymerase chain reaction (RT-PCR) and immunohistochemistry (IHC).

Findings: Five patients were included, one male and four female, aged 7 months to 15 years. Two patients had severe diseases before SARS-CoV-2 infection: adrenal carcinoma and Edwards syndrome. Three patients were previously healthy and had multisystem inflammatory syndrome in children (MIS-C) with distinct clinical presentations: myocarditis, colitis, and acute encephalopathy with status epilepticus. Autopsy findings varied amongst patients and included mild to severe COVID-19 pneumonia, pulmonary microthrombosis, cerebral oedema with reactive gliosis, myocarditis, intestinal inflammation, and haemophagocytosis. SARS-CoV-2 was detected in all patients in lungs, heart and kidneys by at least one method (RT-PCR, IHC or EM), and in endothelial cells from heart and brain in two patients with MIS-C (IHC). In addition, we show for the first time the presence of SARS-CoV-2 in the brain tissue of a child with MIS-C with acute encephalopathy, and in the intestinal tissue of a child with acute colitis. Interpretation: SARS-CoV-2 can infect several cell and tissue types in paediatric patients, and the target organ for the clinical manifestation varies amongst individuals. Two major patterns of severe COVID-19 were observed: a primarily pulmonary disease, with severe acute respiratory disease and diffuse alveolar damage, or a multisystem inflammatory syndrome with the involvement of several organs. The presence of SARS-CoV-2 in several organs, associated with cellular

---

* Corresponding author at: Faculdade de Medicina da Universidade de São Paulo, Departamento de Patologia. Av. Dr. Arnaldo, 455, sala 1155 – Cerqueira Cesar, Sao Paulo, SP 01246-903, Brasil.
  E-mail address: maridol@usp.br (M. Dolhnikoff).
  [1] A.N.D.N. and E.G.C. contributed equally to this work.

ultrastructural changes, reinforces the hypothesis that a direct effect of SARS-CoV-2 on tissues is involved in the pathogenesis of MIS-C.

Research in context

Evidence before this study

We searched PubMed for studies describing the pathology of COVID-19 in children, published in any language, until October 19, 2020. The search terms were "COVID-19″ OR "SARS-CoV-2″ AND "Autopsy" AND "Children". We found two articles that describe autopsy findings in children with COVID-19. A case report describes a 17-year-old African American with sudden extra-hospital death. The autopsy showed diffuse eosinophilic interstitial myocarditis, pulmonary congestion and haemorrhage, mild bronchitis, and hepatic congestion. Another case report describes a 19-week-old stillborn, whose mother acquired COVID-19 and had a miscarriage. The placenta tested positive for SARS-CoV-2-RNA, but foetal tissues were negative. The histology showed acute funisitis, acute subchorionitis, intervillous fibrin deposition, and syncytial knots.

Added value of this study

We describe the pathology findings in five children and adolescents who died with COVID-19 (7 months to 15 years old), representing the world's largest autopsy study addressing this issue to date. Tissue samples from all vital organs (lungs, heart, brain, kidneys, liver, and spleen) were analysed by histology, electron microscopy (EM), reverse-transcription polymerase chain reaction (RT-PCR) and immunohistochemistry (IHC). A myriad of clinical-pathological presentations was found. Two patients had other severe diseases previous to SARS-CoV-2 infection: one adolescent with adrenal carcinoma, who had diffuse alveolar damage (DAD) and thrombotic events, and an infant with Edwards syndrome, with severe COVID-19-related pneumonia, DAD, and syncytial giant cell hepatitis attributed to SARS-CoV-2 infection. Three other patients fulfilled the criteria for MIS-C, and all of these had extrapulmonary manifestations attributed to SARS-CoV-2 infection (myocarditis, colitis, and acute encephalopathy with status epilepticus). Autopsy findings varied amongst patients and included mild to severe COVID-19 pneumonia, pulmonary microthrombosis, cerebral oedema with reactive gliosis, myocarditis, intestinal inflammation, and haemophagocytosis. SARS-CoV-2 RNA, antigens and virions were detected in several tissues by RT-PCR, IHC and EM, respectively. In all patients, SARS-CoV-2 was detected in lungs, heart and kidneys by at least one method (RT-PCR, IHC or EM).

Implications of all the available evidence

In this series of five children, we observed patients with a primarily pulmonary disease, with severe acute respiratory disease and DAD, and patients with a multisystem inflammatory syndrome, with the involvement of several organs. We show evidence that SARS-CoV-2 has a great invasive potential, infecting several organs and endothelial cells. In particular, we show for the first time the presence of SARS-CoV-2 in the brain tissue of a child with MIS-C with acute encephalopathy, and in the intestinal tissue of a child with acute colitis. The local tissue inflammatory response is variable, and the target organ for the predominant clinical manifestation varies amongst individuals.

The presence of SARS-CoV-2 in several organs, associated with cellular ultrastructural changes, reinforces the hypothesis that a direct effect of SARS-CoV-2 on tissues is involved in the pathogenesis of MIS-C.

1. Introduction

Children and adolescents are the age group with the lowest risk of severe presentation and complications from COVID-19 [1]. They account for 1 to 8% of laboratory-confirmed cases and less than 1% of the total number of deaths [2−4]. Most children have asymptomatic or mild disease and recover within a few weeks of disease onset, a small proportion develop severe disease, requiring paediatric intensive care unit (PICU) admission and prolonged ventilation [3,5].

The clinical presentation of COVID-19 in children is variable. In a European series of 582 children and adolescents, 8% of individuals developed severe disease, 52% were associated with pre-existing medical conditions, and most had a clinical-radiological presentation of pneumonia and/or acute respiratory distress syndrome (ARDS) [1]. In a systematic review of SARS-CoV-2 infection in children and newborns, 2% had severe disease and were admitted to the PICU unit with dyspnoea, cyanosis and hypoxaemia [6]. Ten patients (0.6%) were critical, and six patients (0.08%) died [6]. Data on COVID-19 in Brazilian children are scarce, despite the fact that Brazil ranks third in number of cases and second in number of deaths. By the end of December 2020, Brazil had registered more than 7.6 million infected people and 193.9 thousand deaths. Amongst these, 1203 children and adolescents died of COVID-19 (0.6%) [7].

Since April 2020, a new childhood inflammatory disorder related to COVID-19 has been reported in many countries. The U.S. Centre for Disease Control and Prevention (CDC) and the World Health Organization (WHO) have distinct but similar definitions of the disorder, named multisystem inflammatory syndrome in children (MIS-C), or paediatric inflammatory multisystem syndrome (PIMS) [8−10]. MIS-C usually occurs two to four weeks after infection with SARS-CoV-2, and critical illness develops in some patients, with prominent cardiac involvement and coronary-artery aneurysms in 10 to 20% of the cases [10]. Patients have elevated levels of inflammatory markers and troponin, especially those with cardiac dysfunction [10]. Most patients recover with intensive care support and estimated mortality is 2 to 4% [10].

The mechanism of systemic disease and the role of SARS-CoV-2 infection in the clinical manifestation of multiple organ involvement are not fully understood. During this pandemic, autopsies have been a valuable tool for understanding the mechanisms involved in tissue injury caused by SARS-CoV-2. To date, reports on the pathology of fatal COVID-19 in children are rare, so this report may help elucidate the extent of the disease, the systemic changes related to the inflammatory syndrome, and the role of virus-induced tissue damage [11−13].

We have recently reported the autopsy findings of an 11-year-old child with MIS-C, and showed that the direct effect of SARS-CoV-2 infection on cardiac tissue was a major contributor to myocarditis and heart failure [11]. In the present study, we extended our investigation to a series of 5 paediatric patients that died of COVID-19 and whose families consented to autopsy. Our findings evidenced two

major patterns of COVID-19 in children and adolescents who died with the disease - a primarily pulmonary disease, and MIS-C with distinct clinical-pathological presentations.

2. Methods

This study was approved by the HC−FMUSP Ethical Committee (protocol no. 3951.904). From 18 March 2020 to 15 August 2020, 3345 patients with confirmed COVID-19 were hospitalized in our institution, with 1219 deaths (mortality rate of 36%). Eighty-two patients were under 20 years old, and 10 died. During this period, we performed 68 autopsies of patients who died with COVID-19, five of whom were children or adolescents. The cases fulfilled the following requirements: ethical board approval, written consent from the next-of-kin, the autopsies had been requested by the clinical staff, and there was availability of the minimally invasive autopsy team. The autopsy of other five patients under 20 years old was not performed, either because the clinical staff did not request the autopsy or because there was no family consent.

Confirmed cases of COVID−19 were defined according to the WHO as those with laboratory confirmation of SARS-CoV-2 infection, regardless of clinical signs and symptoms [9]. Demographic and clinical data were retrieved from medical charts. Echocardiograms were performed on all patients according to the guidelines of the American Society of Echocardiography (ASE) [14]. Coronary arteries were evaluated according to the American Heart Association Statement for Diagnosis, Treatment and Long-Term Management of Kawasaki Disease [15]. Dilation was diagnosed whenever the coronary artery internal lumen diameter z-score was greater than +2.5 [15].

Ultrasound-guided minimally invasive autopsy (MIA-US) was performed with tissue sampling of the heart, lungs, liver, spleen, kidneys, brain, quadriceps muscle and skin of all the patients. As minimally invasive autopsy is not the ideal method for sampling the intestine, adequate intestinal samples were obtained from two patients only (patients 2 and 4). Bone marrow was also collected from patients 2 and 4, and parotid tissue from patients 4 and 5. We used a portable SonoSite M−Turbo R (Fujifilm, Bothell, WA, USA) ultrasound equipment and Tru−Cut semi−automatic coaxial needles (14 G; 20 cm in length) for tissue sampling, a 5−mm skin-punch needle, and trans−sphenoidal puncture to access the brain [16].

Immunohistochemistry (IHC) was performed on all collected tissues to detect SARS-CoV-2 antigens: Nucleocapsid protein (mouse monoclonal antibody [6H3] -GeneTex Inc., Irvine, CA, USA, 1:500 dilution) and Spike protein (MP Biomedicals, Irvine, Califórnia, USA, 1:1000 dilution). The primary antibodies were tested in lung samples from patients with Influenza H1N1 pneumonia, measles, syncytial respiratory virus, herpes virus, cytomegalovirus, and adenovirus, obtained from our autopsy archive. The IHC reaction resulted negative in all these samples. Adult pulmonary tissue with SARS-CoV-2 pneumonia was used as positive control. Detailed IHC protocol is presented in appendix p.4. IHC for glial fibrillary acidic protein (GFAP) (2GF2, Dako, Via Real Carpinteria, CA, USA, 1:500 dilution); CD45 (PD7/26, DAKO, 1:2000) and CD68 antigens (PG-M1, Dako, 1:2500 dilution) was performed on brain tissue, and C4d (SP91, Abcam, Cambridge, UK, 1:200 dilution) on heart tissue for identification of cardiomyocyte necrosis. The antigen retrieval was done with citrate at pH 6.0 for GFAP, CD45 and with Tris-EDTA, pH 9.0, for C4d and CD68.

Tissue samples from all patients were examined under transmission electron microscope (EM). For patients 1 to 4, samples of the lungs and heart were retrieved from paraffin blocks from specific areas with altered histology. As patient 4 had important abdominal symptoms, a sample of intestinal tissue was also retrieved from the paraffin block of this patient. For patient 5, samples from the lungs, heart and brain were collected and fixed in 2% glutaraldehyde. The tissue samples retrieved from the paraffin blocks were submitted to xylol deparaffinization and tissue rehydration in graded alcohol series, followed by re-fixation in glutaraldehyde. All samples were post-fixed in 1% OsO$_4$, stained in 1% aqueous uranyl acetate, and embedded in epoxy resin. Ultrathin sections were double-stained by uranyl acetate and lead citrate. For patient 5, we also performed immunogold labelling for SARS-CoV-2 (detailed protocol in appendix p.6). Micrographs were obtained with a Jeol JEM 1010 electron microscope (Tokyo, Japan, 80 kV).

Real Time RT-PCR was employed for molecular detection of SARS-CoV-2 in pulmonary and heart tissues of all patients and in intestinal tissue and parotid gland of patient 4. Tissues were submitted to homogenization using the FastPrep^{TM} instrument (MP Biomedical; São Caetano do Sul, SP, Brazil) and nucleic acid extraction was performed using the TRIzol$^®$ reagent (Invitrogen, Carlsbad, CA, USA). Molecular detection of SARS-CoV-2 was performed using Super-Script^{TM} III Platinum^{TM} One-Step qRT-PCR Kit (Invitrogen) with primers and probes described in the CDC and Charité protocols that amplify the region of the nucleocapsid N gene (2019_nCoV_N1 assay) [17] and E gene (E_Sarbeco assay) [18], respectively. Human RNase P gene was also amplified as nucleic acid extraction control [17,18]. The reactions were carried out in a 7500 Fast Real-Time PCR System (Applied Biosystems, Foster City, CA, USA) and consisted of a step at 50 °C for 15 min for the reverse transcription, followed by incubation at 95 °C, for 2 min, and 45 cycles of temperature varying from 95 °C for 15 s to 55 °C (N and RNAse P genes)/ 58 °C (E gene) for 30 s.

Role of the funding source: The sponsors of the study had no role in study design; in the collection, analysis, and interpretation of data; in the writing of the report; and in the decision to submit the paper for publication. All authors had full access to all the data in the study and assumed the final responsibility to submit this manuscript for publication.

3. Results

Five children and adolescents who died with COVID-19 were autopsied, aged from 7 months to 15 years old. The post-mortem interval for tissue collection ranged from 8 to 14 h. Patients 1 and 2 had severe diseases before SARS-CoV-2 infection and presented a pulmonary form of COVID-19. Patients 3 to 5 were previously healthy, and fulfilled the WHO/CDC criteria for MIS-C (appendix p.1). Tables 1, 2 and 3 show clinical, laboratory and pathological characteristics, respectively, for each patient. Appendix p.4 and p.5 show additional IHC results.

Patient 1 was a 15-year-old female adolescent with secondary amenorrhoea and abdominal distension. During hospitalization, an adrenal carcinoma associated with a mutation in the PT53 gene was diagnosed. This cancer produced testosterone and aldosterone, and there were pleural and peritoneal metastases. The patient acquired COVID-19 in the hospital, developing a fever and a cough, but the chest computerized tomography (CT) did not find typical SARS-CoV-2 pneumonia. She developed a secondary bacterial pneumonia and empyema, requiring a thoracic drain. Oxacillin-susceptible *Staphylococcus lugdunensis* was identified in the pleural fluid culture. The patient developed acute kidney injury and received substitutive renal therapy. Thrombosis was detected by CT in the inferior vena cava, mesenteric veins and renal veins. The patient progressed to respiratory failure with refractory hypoxaemia and progressive shock and was considered for palliative care, dying 5 days after the diagnosis of COVID-19. The patient did not meet MIS-C criteria because she had an alternative diagnosis for the clinical condition, that is, advanced neoplasia and empyema. The main autopsy findings were foci of exudative diffuse alveolar damage (DAD), fibrin thrombi in the pulmonary arteries and in the liver, foci of suppurative secondary pneumonia, and hepatic ischaemic necrosis (Fig. 1, Table 3).

Patient 2 was a 7-month-old preterm, low birth-weight female infant (33 weeks gestation and 1565 g at birth) with trisomy 18 (Edwards syndrome), foramen ovale and two ventricular muscular

Table 1
Clinical features and image exams.

Characteristics	Patient 1	Patient 2	Patient 3	Patient 4	Patient 5
Sex, age Ethnicity BMI, kg/m^2 (z-score)	F, 14 to 17 yo White 27.1 (+1.9) Overweight	F, < 1 yo White 11.2 (< −3) Undernourished	F, 8 to 12 yo African descent 22.6 (+ 1.5) Overweight	M, 8 to 12 yo African descent 23.6 (> + 3) Obese	F, 8 to 12 yo African descent 21.24 (> +2) Obese
Onset of symptoms to death (days)	24	12	8	10	28
Hospitalization (days)	9	7	1	6	24
SARS-CoV-2 infection diagnosis	Positive NP/OP swab RT-PCR	Positive NP/OP swab RT-PCR	Positive NP/OP swab RT-PCR (the result was only available after death) Positive post-mortem NP/OP swab RT-PCR, collected at autopsy	Negative NP/OP swab RT-PCR, positive serology (the result was only available after death) Positive post-mortem tissue RT-PCR	Clinical suspicion, negative NP/OP swab RT-PCR, negative serology (post-mortem serology with stored blood) Post-mortem identification of SARS-CoV-2 by EM and IHC
Chest computed tomography scan	Bilateral pleural effusion, mainly on left side	Bilateral and extensive ground-glass opacities Air-bronchograms	Multiple ground-glass opacities, sparse bilateral foci of consolidation, mainly in the peripheral and posterior areas of the lower lobes	Ground-glass opacities and consolidations, mainly in posterior areas of the left lower lobe Mild left pleural effusion	Few and small foci of ground-glass opacities
Echocardiogram	Small pericardial effusion, echogenic mass in the inferior vena cava and right atrium (metastatic tumour), preserved LVEF (71%), normal coronary arteries	Patent foramen ovale, two small apical ventricular septum defects (2.5 and 1.7 mm), bicuspid aortic valve without dysfunction, preserved LVEF (64%), normal coronary arteries	Small pericardial effusion, LV global hypokinesis with reduced EF (30%), normal coronary arteries	Dilated LV, with global hypokinesis and reduced EF (35%). RV systolic dysfunction (TAPSE = 1.1 cm), normal coronary arteries	Preserved LVEF (60%), hyperechogenic coronary arteries, right coronary artery diffuse ectasia (z-score = +3), left anterior descending coronary artery diffuse ectasia (z-score = +2.6)
Treatment	Ceftriaxone, azithromycin, piperacillin/tazobactam, vancomycin, hydroxychloroquine and heparin	Ceftriaxone, azithromycin, oseltamivir and methylprednisolone	Ceftriaxone, azithromycin	Ceftriaxone, metronidazole, clarithromycin, vancomycin, meropenem, oseltamivir, and two doses of intravenous immunoglobulin, due to the hypothesis of MIS-C	Thiopental, phenytoin and levetiracetam; acyclovir to treat presumptive viral meningoencephalitis; pulse therapy with methylprednisolone and gamma globulin for severe MIS-C, ceftriaxone; piperacillin/tazobactam, vancomycin

Abbreviations: F: female; M: male; yo: years old; mo: months old; NP/OP: Nasopharyngeal/oropharyngeal; RT-PCR: reverse transcription-polymerase chain reaction; LVEF: left ventricular ejection fraction; LV: left ventricle; RV: right ventricle; TAPSE: tricuspid annular plane systolic excursion; EF: ejection fraction; MIS-C: Multisystem inflammatory syndrome in children; IHC: immunohistochemistry; EM: electron microscopy.

septal defects, measuring 2.5 and 1.7 mm. She also presented with cholestasis and was discharged three months after birth, receiving both breast and bottle feeding with no cardiovascular medication. Immunoglobulins G and M against cytomegalovirus and herpesvirus were positive. The patient returned four months after discharge with nasal congestion, respiratory distress and worsening of cholestasis, without fever, cough or gastrointestinal (GI) symptoms. The RT-PCR of nasal secretions detected rhinovirus and SARS-CoV-2 infections. The chest CT showed extensive bilateral consolidations and ground-glass opacities (Fig. 2A). The patient progressed to respiratory failure requiring ventilatory support. At this point, the echocardiogram indicated signs of severe pulmonary hypertension and treatment with nitric oxide and milrinone was started. The infant progressed to refractory hypoxaemia and multi organ failure, and died 12 days after hospitalization. Nosocomial infection was ruled out. The main autopsy findings were a typical COVID-19 pneumonia with diffuse alveolar damage, cholestatic hepatitis with syncytial giant cells and haemophagocytosis in the bone marrow (Fig. 2B-F, Table 3). This case was considered as a severe SARS-CoV-2 pneumonia, decompensating the previous congenital heart disease and neonatal cholestatic hepatitis.

Patient 3 was a previously healthy 11-year-old female child, who died due to MIS-C related to SARS-CoV-2 infection, with a 10-day course of illness and one day of hospitalization. She had persistent fever, odynophagia, myalgia, abdominal pain, mild respiratory distress, severe cardiac dysfunction, and refractory shock. The nasopharyngeal RT-PCR for SARS-CoV-2 collected during hospitalization was positive (the result was only available after death). Serology was not performed. The patient had previous contact with a relative with COVID-19. The autopsy showed diffuse cardiac inflammation, with myocarditis, endocarditis and pericarditis, microthrombi in the lungs and glomerular tufts, haemophagocytosis and mild COVID-19 pneumonia. This case was previously described in detail; we showed that the myocarditis was induced by SARS-CoV-2, which was detected by EM in several cardiac cells [11]. In the present report, we add the EM findings in the pulmonary tissue, as well as the immunohistochemistry analysis, which detected SARS-CoV-2 antigen in all vital organs (Fig. 3, Table 3).

Patient 4 was a previously healthy 8-year-old male child, with a past history of mild asthma, sickle cell trait and obesity, admitted with a 4-day history of fever and abdominal pain. He arrived at the hospital with fever, abdominal pain, tachycardia, and tachypnoea. In

Table 2
Laboratory results.

Analyte*	Patient 1	Patient 2**	Patient 3	Patient 4	Patient 5	Reference Range
Haemoglobin (g/dL)	10.5/12.2	10.9/9.8	10.0/11.0	8.8/7.3	11.7/9.0	12.7 - 14.7 g/dL
Haematocrit (%)	32.7/39.0	30.7/28.8	28.8/33.0	25.6/21.4	35.6/25.0	38 - 44%
Leukocytes, x10³ cells per mm³	9.30/23.60	32.95/60.18	25.73/38.22	14.04/14.18	9.31/4.70	$4.5 - 4.4 \times 10^3$ cells per mm³ **$6-18 \times 10^3$ cells per mm³
Neutrophils (percentage of total WBC)	81/93	28/83	74/63	95/85	84/37	40−75
Lymphocytes (percentage of total WBC)	9/3	58/15	4/9	3/13	5/55	20−45
Platelets × 10³ cells per μL	383/172	496/96	167/145	111/30	182/241	150 − 450 × 10³ cells per μL
Urea (mg/dL)	122/127	23/42	67/93	29/160	60/87	11 − 38 mg/dl **10−50 mg/dL
Creatinine (mg/dL)	1.87/ 4.53	0.26/1.03	1.27/2.19	0.52/3.74	0.73/2.01	0.53 - 0.79 mg/dL **0.17−0.42 mg/dL
Troponin T (ng/mL)	0.0024/0.037	0.008/0.385	0.281/0.342	0.0128/5.462	0.011/0.010	<0.014 ng/mL
CPK (U/L)	60/231	1008/−	96	−/47,557	50/18	<167 U/L
CKMB (ng/mL)	2.87/−	30.71	5.76/15.66	− /19.70	0.64/1.07	0.1 − 2.88 ng/mL
D-dimer (ng/mL FEU)	2324/15,181	323/29,030	11,495/54,153	>10,000/>10,000	1041/543	<500 ng/mL
Fibrinogen (mg/dL)	269	111/90	513	399/399	356/424	200 − 393 mg/dL
INR	1.23/3.13	1.0/1.25	1.40	1.28/1.80	1.14/1.35	0.9 - 1.2
aPTT (s)	36.0/46.3	40.9/48.8	−	57.9/50.3	37.2/36.5	25.4−38.9 **25.1−36.5
C-reactive protein (mg/L)	190/−	1.5/1.3	266.6/309.5	181/248	8.5/33.4	<5 mg/L
Ferritin (ng/mL)	295	1119	1501	− /3422	159	20 − 200 ng/mL
Albumin (g/dL)	2.4/2.0	4.3/3.3	2.6	2.5/2.4	2.9/2.6	3.8 - 5.4 g/dL **3.4−3.9 g/dL
Triglycerides (mg/dL)	59/−	205	162	−/−	272	100−129 mg/dL
Aspartate aminotransferase (U/L)	290/4650	506/279	61/67	41/88	112/41	13 − 35 U/L **9−80 U/L
Alanine aminotransferase (U/L)	376/3338	367/217	67/67	36/50	69/51	7 − 35 U/L **13−45 U/L
Gamma glutamyl transferase (U/L)	191/351	479/398	85	409/2015	59/646	3−20 U/L **5−36 U/L
Alkaline phosphatase (U/L)	151/273	469/225	−/−	198/106	357/177	129−417 U/L **<187 U/L
Lactate dehydrogenase (U/L)	>6000	375/3646	40 / 47	757/−	585	120−300 U/L
Total bilirubin (mg/dL)	0.33/2.05	11.07/12.76	0.29	5.47/2.39	0.38	<0.9 mg/dL
Direct bilirubin (mg/dL)	0.29/ 1.98	9.84/11.51	0.23	3.86/1.80	0.37	<0.2 mg/dL **<0.3 mg/dL
Lactate (mg/dL)	39/67	28/150	38/29	16.8/91.8	14/25	4.5 −14.4 mg/dL

*The values for each analyte, in each cell, represent the first and last results during hospitalization (analyte value in the first 48 h of hospitalization / analyte value in the last 48 h of life).
**Reference range for laboratory results for patient 2.
Abbreviations: INR: prothrombin international standardized ratio; aPTT: Activated partial thromboplastin time; CPK: creatine phosphokinase; CKMB: creatine kinase myocardial band; WBC: white blood cells.

the first hours in the emergency room, he remained haemodynamically stable, but with worsening abdominal pain. The initial diagnosis was acute inflammatory abdomen. Appendicitis or COVID-19-related acute abdomen were considered as possible diagnoses. He had no respiratory symptoms but mild chest CT alterations were observed, mainly in the lower left lobe (Fig. 4A). He underwent an emergency laparotomy and developed intraoperative shock. The surgical findings were a small amount of non-purulent fluid in the peritoneal cavity, and a hyperaemic and oedematous appendix. Even without the presence of typical appendicitis, removal of the appendix was done as the only procedure option at that time. Haemoculture and culture of abdominal fluid were negative. In the postoperative period, the patient developed respiratory distress, persistent fever (up to 41.1 °C), global cardiac dysfunction with worsening of shock and inflammatory test results. Patient progressed to multiple organ dysfunction from the 8th day of illness and died on the 10th day. The nasopharyngeal RT-PCR for SARS-CoV-2 collected during hospitalization was negative. The serology was positive (IgG positive, IgM negative, ELISA assay; Neutralizing antibody titre: 1:640, [range 1/20 - 1/2150]), but the result was only available after death. There was no history of exposure to SARS-CoV-2. The main autopsy findings were colitis with predominantly lymphocytic infiltration, and detection of SARS-CoV-2 antigens in the intestinal glands; focal exudative DAD; glomerular microthrombi, and a severe contraction band necrosis in the myocardium (Fig. 4, Table 3).

Patient 5 was a previously healthy 8-year-old female child who had odynophagia, high fever (41 °C) and headache, who progressed in five days to adynamia, vomiting, altered consciousness and status epilepticus. She was treated with anticonvulsants and subjected to mechanical ventilation. The cerebrospinal fluid showed a mild increase in cell count. The electroencephalogram (EEG) confirmed the status epilepticus and the chest CT showed small foci of ground-glass infiltrates. On the 10th day of illness, a ventilator-associated pneumonia due to oxacillin-resistant *S. aureus* was detected. On the 14th day, the transcranial Doppler showed loss of cerebral autoregulation and spasm on the left middle cerebral artery. From the 17th to the 22nd day, she maintained seizures on the EEG, despite the optimization of the anticonvulsants. On the 27th day of illness, she developed refractory shock and severe acidosis, and died. The nasopharyngeal RT-PCR for SARS-CoV-2 collected during hospitalization was negative. Serology was not performed. There was no history of exposure to SARS-CoV-2. The main autopsy findings were cerebral oedema, with the presence of SARS-CoV-2 antigens in cerebral endothelial cells and in the perivascular astroglial cells by IHC, diffuse pulmonary microthrombosis, and haemophagocytosis (Figs. 5 and 6, Table 3, and appendix p.5 panels D and E).

All patients received intensive care from specialized paediatricians, mechanical ventilation, vasoactive drugs, and antimicrobials (Table 1). Table 2 shows the laboratorial work-up of all patients, indicating, in general, anaemia, lymphopenia, acute kidney injury,

Table 3
Autopsy findings.

Organ	Patient 1	Patient 2	Patient 3	Patient 4	Patient 5
Lungs	Foci of DAD Foci of bacterial pneumonia Congestion, oedema, foci of haemorrhage Thrombi in arterial vessels and septal capillaries. Angiomatoid pattern. Rare cells with cytopathic change Large number of megakaryocytes	*Typical SARS-CoV-2 pneumonia with exudative DAD No thrombi	Congestion, oedema, foci of haemorrhage Thrombi in arterial vessels and septal capillaries. Rare cells with cytopathic change Large number of megakaryocytes	Congestion, oedema, foci of haemorrhage Rare cells with cytopathic change Foci of exudative DAD Thrombi in septal capillaries	Congestion, oedema, foci of haemorrhage Thrombi in arterial vessels and septal capillaries Angiomatoid pattern. Various foci of coagulative necrosis Rare cells with cytopathic change
Heart	Interstitial oedema	Interstitial oedema	Pericarditis, myocarditis, endocarditis, myocardial necrosis	Small foci of myocarditis, diffuse band necrosis, interstitial oedema	Foci of band necrosis, interstitial oedema
Liver	Congestion, centrilobular necrosis, arterial thrombi with ischaemic necrosis	Congestion, cholestasis, centrilobular necrosis, syncytial metaplasia of hepatocytes	Congestion, centrilobular necrosis, sinusoids thrombi Haemophagocytosis by Kupffer cells	Congestion, micro/macrovesicular steatosis, multinucleation, mild portal infiltrate	Congestion, hepatocyte binucleation
Kidneys	ATN, congestion, nephrocalcinosis, mesangial cell hyperplasia	ATN, congestion	ATN, congestion, fibrin thrombi in glomerular capillaries	ATN, congestion, fibrin thrombi in glomerular capillaries, tubular hyaline casts	ATN, congestion, exudate in the Bowman space, granular casts
Spleen	Splenitis, haemorrhages, lymphoid hypoplasia with reactive cells	Splenitis, haemorrhages, lymphoid hypoplasia with reactive cells	Splenitis, haemorrhages, lymphoid hypoplasia with reactive cells Haemophagocytosis Sinusoidal fibrin thrombi	Splenitis, haemorrhages, lymphoid hypoplasia	Splenitis, haemorrhages, lymphoid hypoplasia with reactive cells Haemophagocytosis
Brain	Reactive microglia, neuronal ischaemia, congestion	Reactive microglia, neuronal ischaemia, congestion	Reactive microglia, neuronal ischaemia, congestion	Reactive microglia, neuronal ischaemia, congestion, oedema Capillary fibrin thrombi	Reactive microglia, neuronal ischaemia, Alzheimer type II glial cells, congestion, oedema
Bone marrow	Not sampled	Hypercellular, haemophagocytosis, emperipolesis by megakaryocytes	Not sampled	Normocellular, normomaturative Mild nuclear atypia of megakaryocytes	Not sampled
Colon	Not sampled	Oedema and mild inflammation	Not sampled	Colitis with dense inflammatory cell infiltration, arteriolar microthrombi, peritonitis Appendicitis with peritonitis (surgical specimen)	Not sampled
Skin	Inadequate sample	Normal	Superficial perivascular mononuclear infiltrate	Superficial perivascular mononuclear infiltrate	Superficial perivascular and periadnexal mononuclear infiltrate
Muscle	Myolysis, necrotic fibres	Myolysis, necrotic fibres	Myolysis, necrotic fibres	Focal myositis	Myolysis, necrotic fibres
Other	Adrenal carcinoma with intense necrosis	—–	Pulmonary lymph nodes with lymphoid hypoplasia and haemophagocytosis	Parotiditis	Parotiditis
Positive IHC for SARS-CoV-2 antigen	Bronchiolar epithelium and rare type 2 pneumocytes; cardiomyocytes and aorta (tunica media); hepatocytes; epithelial tubular cells; spleen (mononuclear cells in the red/white pulp); perivascular astrocytes; fat tissue and nerves	Bronchiolar cells, airway submucosal glands; cardiomyocytes, cardiac endothelial cells; hepatocytes; renal epithelial tubular cells; microglia; bone marrow mononuclear cells	Bronchiolar and rare alveolar cells, pulmonary megakaryocytes; cardiomyocytes and cardiac endothelial cells; hepatocytes and biliary tract epithelium; renal epithelial tubular cells; spleen (mononuclear cells in the red/white pulp); brain endothelial cells; sweat glands and subcutaneous nerves; fat tissue	Bronchiolar and rare alveolar cells, airway submucosal glands; cardiomyocytes and cardiac endothelial cells; hepatocytes; renal epithelial tubular cells; spleen (mononuclear cells in red/white pulp); intestinal epithelium; Peyer's patch macrophages, brain (microglia and endothelial cells); sweat glands; parotid ductal and acinar cells; fat tissue and nerves	Few bronchiolar and alveolar cells; cardiomyocytes and cardiac endothelial cells; hepatocytes; renal epithelial tubular cells; spleen (mononuclear cells in red/white pulp; brain (microglia, endothelial cells, perivascular astrocytes); parotid ductal and acinar cells
EM findings	Desquamation of pneumocytes, endothelial changes in heart and lung Viral particles in sites of marked pathological changes: in desquamated pneumocytes and amongst ruptured sarcomeres in cardiomyocytes	Type 2 pneumocytes with numerous short microvilli at the luminal surface; septal vessels with tiny fibrin clots; rupture of endothelial cells Viral particles in pneumocytes and cardiomyocytes	Lung: desquamation of pneumocytes and denudation of the basal membrane. Viral particles in endothelial cells See ref. [11] for EM in heart tissue	Cytopathic alterations and presence of viral particles in alveolar epithelium, cardiomyocytes, and intestinal smooth muscle cells	Lung with desquamation of pneumocytes, rupture of endothelium, viral particles on the alveolar surface Brain with viral particles in the endothelium and in astrocytes, disorganization of blood-brain barrier, capillary lumen filled with fibrin

Table 3 (*Continued*)

Organ	Patient 1	Patient 2	Patient 3	Patient 4	Patient 5
					Viral particles in cardiomyocytes
RT-PCR for SARS-CoV-2 in tissues (N1 and E assays) §	Positive in lung (34/37) and heart (29/30)	Positive in lung (15/17) Negative in heart	Positive in lung (33/36) and heart (34/36)	Negative in lung and heart Positive in intestine (35/37) and parotid (37/38)	Negative in lung and heart
Immediate cause of death Underlying cause of death	Disseminated thrombosis Adrenal carcinoma, suppurative pneumonia, and COVID-19	COVID-19 pneumonia Edwards syndrome	SARS-CoV-2 Myocarditis MIS-C/COVID-19	SARS-CoV-2 Colitis MIS-C/COVID-19	SARS-CoV-2 Meningoen-cephalitis MIS-C/COVID-19

DAD: diffuse alveolar damage; ATN: acute tubular necrosis; IHC: immunohistochemistry; EM: electron microscopy; RT-PCR: reverse transcription-polymerase chain reaction.
§ Cycle threshold of each assay is shown in parenthesis (N1/E).
*Typical SARS-CoV-2 pneumonia: reactive epithelial atypia, hyperplasia of type 2 pneumocytes, diffuse alveolar damage, foci haemorrhage, septal oedema.

elevated troponin and D-dimer, low serum albumin, hypoxia and lactic acidosis. High levels of transaminases were observed in patient 1, with hepatic thrombosis, and, in patient 2, with syncytial hepatitis. For all the patients, a panel of PCR (Filmarray®; bioMérieux, Jacarepagua, RJ, Brazil) for other viruses (influenza, parainfluenza, syncytial respiratory virus, metapneumovirus, parechovirus, adenovirus,

rhinovirus, bocavirus and coronavirus), as well as for *Mycoplasma pneumoniae*, was performed on respiratory secretions at admission. The results were negative, except for case 2 (positive for rhinovirus).

Table 3, Figs. 1 to 6, and appendix p.4 and p.5 show that IHC for SARS-CoV-2 antigen was positive in all patients, in several tissues. IHC detected high density of CD68 positive cells in brain tissue in all cases with focal distribution in the meninges in three cases (patients 3, 4, and 5), corroborating the finding of microglial reactivity. EM evidenced viral particles in heart and lungs in all patients, in intestine in patient 4, and in the brain tissue in patient 5 (Figs. 1 to 6, Table 3).

4. Discussion

This is the first autopsy series of COVID-19 in children and adolescents. We were able to study the fatal event in patients with and without comorbidities, and with pulmonary and non-pulmonary manifestations of the disease. Our findings show a spectrum of clinical and pathological presentations of severe COVID-19 in this age group.

Severe COVID-19 in children is rare. Most paediatric patients have asymptomatic or mild disease. Our autopsy findings provided mechanistic insight into injury mechanisms in severe cases, which were associated with the viral ability to invade tissues, leading to local effects, or were a consequence of dysregulation of the immune response and/or haemodynamic changes secondary to peripheral infection, or even associated with previous conditions, such as congenital disorders or neoplasms. We suggest that SARS-CoV-2 infection in different tissues, detected by IHC, EM, and RT-PCR, can be interpreted in the context of three possible types of tissue response: I- viral-induced injury with local inflammatory and structural changes, with clinical repercussion (for example: myocarditis and colitis); II- cell infection without local inflammation, but with structural cellular alterations, with clinical repercussion (for example myocardial necrosis without inflammation); and III- cell infection without local inflammation or evident structural alterations, and with no clinical repercussion, which has currently uncertain clinical-pathogenic significance (for example positive SARS-CoV-2 antigen in sweat glands − as found in patients 4 and 5). There seems to be an overlap of these three patterns of tissue response in the same host in different organs.

In this series of five patients, we observed two major patterns of severe COVID-19: a primary pulmonary manifestation, with SARS-CoV-2 pneumonia, observed in patients 1 and 2, or a multisystem inflammatory syndrome with the involvement of several organs and tissues, observed in patients 3 to 5. Other groups have also proposed similar patterns of severe paediatric COVID-19 - a predominant airway/lung disease, and MIS-C [20]. Patients 1 and 2 had severe diseases before SARS-CoV-2 infection, a 15-year-old patient with a terminal neoplastic disease, and a 7-month-old child with Edwards syndrome and a long hospital stay; both presented a pulmonary form
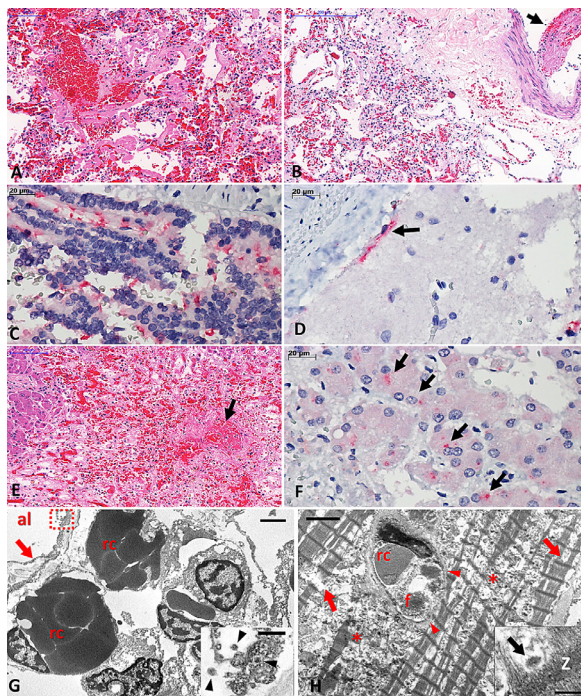

Fig. 1. Pathology of COVID-19 in patient 1. (A) Exudative diffuse alveolar damage with alveolar haemorrhage and hyaline membranes; H&E. (B) Thrombus in a medium sized pulmonary artery (arrow); H&E. (C-D) Detection of SARS-CoV-2 N antigen by IHC in the bronchiolar epithelium (dots in red, C), and perivascular astrocyte (arrow in D). (E) Thrombus in a centrilobular vein (arrow), associated with hepatic ischaemic necrosis and sinusoidal congestion; H&E. (F) Detection of SARS-CoV-2 N antigen by IHC in hepatocytes, in a granular cytoplasmic pattern (arrows). (G) Low magnification electron micrograph of the alveolar wall showing two typical ultrastructural features of SARS-CoV-2 lung infection: congestion of a red blood cell (rc) within a capillary lumen and desquamation of epithelium (arrow) into the alveolar lumen (al). The inset shows viral particles (arrowheads) inside a type 1 pneumocyte, and also in the alveolar lumen. Bar: 2 μm; Inset bar: 500 nm. (H) Low magnification electron micrograph of the myocardium showing several longitudinally cut myofibrils in which the regular striation pattern of the sarcomeres is visible. Some sarcomeres are ruptured (arrows). The asterisks highlight focal areas with more advanced lesions, characterized by massive fragmentation and loss of myofibrils. Also note a capillary with an injured endothelial cell in two points (arrowheads), resulting in direct contact of the myocardial cells with the vascular lumen, filled with red blood cells (rc) and fibrin (f); The inset shows a virus particle (black arrow) in a focal area of ruptured myofilaments at the Z line level (Z). Bar: 2 μm; Inset bar: 200 nm.
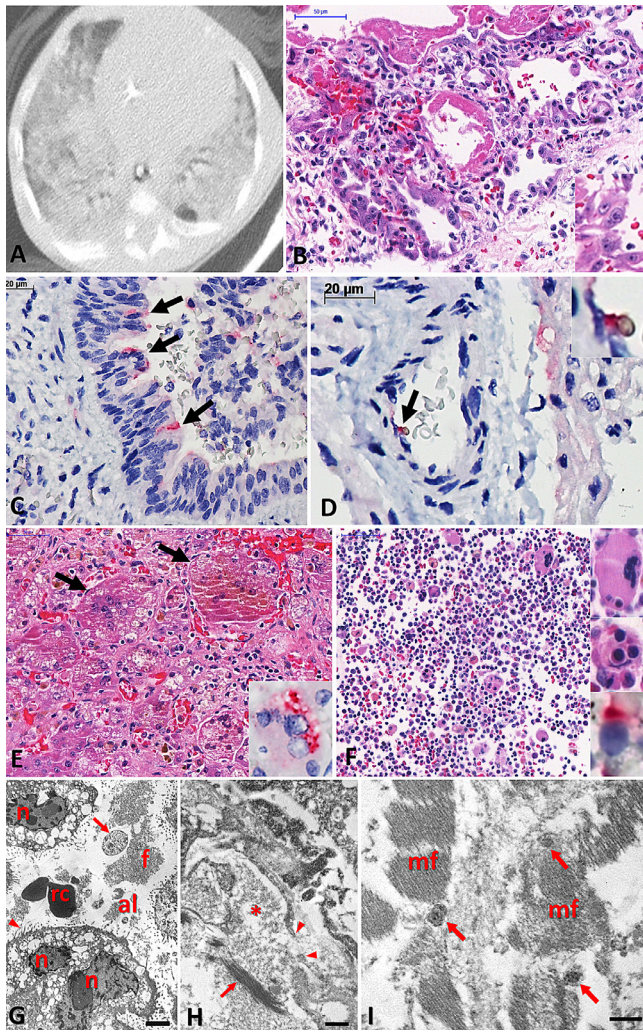
Fig. 2. Pathology of fatal COVID-19 in patient 2. (A) Extensive and bilateral COVID-19-related pneumonia on the chest tomography, with ground-glass opacities, consolidation and air-bronchograms. (B) Typical COVID-19 pneumonia, with type 2 pneumocyte atypia and exudative diffuse alveolar damage; H&E. (C-D) Detection of SARS-CoV-2 N antigen by IHC in the bronchiolar epithelium (arrows in C), and endothelial coronary artery (D, arrow and inset). (E) Giant and multinucleated hepatocytes (arrows), containing bile pigment, and with cytoplasmic detection of SARS-CoV-2 N antigen by IHC (inset). (F) Reactive bone marrow with megakaryocytic emperipolesis, haemophagocytosis by macrophages and positive SARS-CoV-2 N antigen by IHC in mononuclear cells (insets, from top to bottom respectively). (G) Electron micrograph of type 2 pneumocytes in a area of pneumocyte hyperplasia (n, nucleus). Numerous microvilli (arrowhead) are seen on the apical surface of the cells. The alveolar space (al) is filled with red blood cells (rc), clusters of fibrin (f) and cell debris (arrow). Bar: 2 μm. (H) Electron micrograph of a capillary vessel in the alveolar septum. The endothelial cell is ruptured (arrowheads), and the capillary lumen is filled with a fine, dense, granular material (asterisk) and fibrin filaments (arrow). Bar: 500 nm. (I) High magnification electron micrograph showing parts of two cardiomyocytes with viral particles (arrows); mf: myofibrils. Bar: 200 nm.

Fig. 3. Pathology of fatal MIS-C related to COVID-19 in patient 3. (A) Inflammatory infiltration on epicardium, surrounding coronary arteries, and myocardium; H&E. (B-H) Detection of SARS-CoV-2 N antigen by IHC; (B) heart: cardiomyocytes and cardiac endothelium (arrows and inset); (C) lungs: bronchiolar epithelium and pulmonary megakaryocytes (inset); (D) brain: endothelial cells (arrows and inset); (E) spleen: mononuclear cells in a "red dot pattern"; (F) skin: sweat glands and subcutaneous nerves (inset); (G) kidneys: epithelial tubular cells in the centre; (H) liver: main biliary ducts. (I) Electron micrograph shows a capillary inside an alveolar septum. A mononuclear inflammatory cell (nu, nucleus) and red blood cell (rc) are seen in the capillary lumen (cl). The arrowheads point to areas where endothelial cells have been denuded. Note the absence of pneumocytes in the alveolar surface (arrow); dotted lines correspond to Fig. 3J. Bar: 1 μm; (J) The image corresponds to a higher magnification of the area surrounded by dotted lines in Fig. 3I. Ultrastructural examination reveals the presence of viral particles inside the endothelial cell (arrows) and in the septal interstitium (arrowheads); al: alveolar lumen; cl: capillary lumen. Bar: 200 nm.

of COVID-19. In the first case, the acute lung injury and thrombogenic events could not be attributed solely to SARS-CoV-2 infection, but, rather, to an association of multiple pathogenic processes including disseminated neoplasia, COVID-19, and staphylococcal pulmonary infection [19,21]. Both SARS-CoV-2 infection and bacterial pneumonia in this case likely represent clinical complications in a patient with metastatic cancer. In the second case, severe COVID-19 pneumonia was the immediate cause of death. Besides pulmonary injury, the IHC identification of viral antigens indicated a disseminated infection by SARS-CoV-2, with involvement of the heart (endothelial cells), liver (hepatocytes) and bone marrow. Extensive pneumonia with ARDS and respiratory failure has been reported as the main
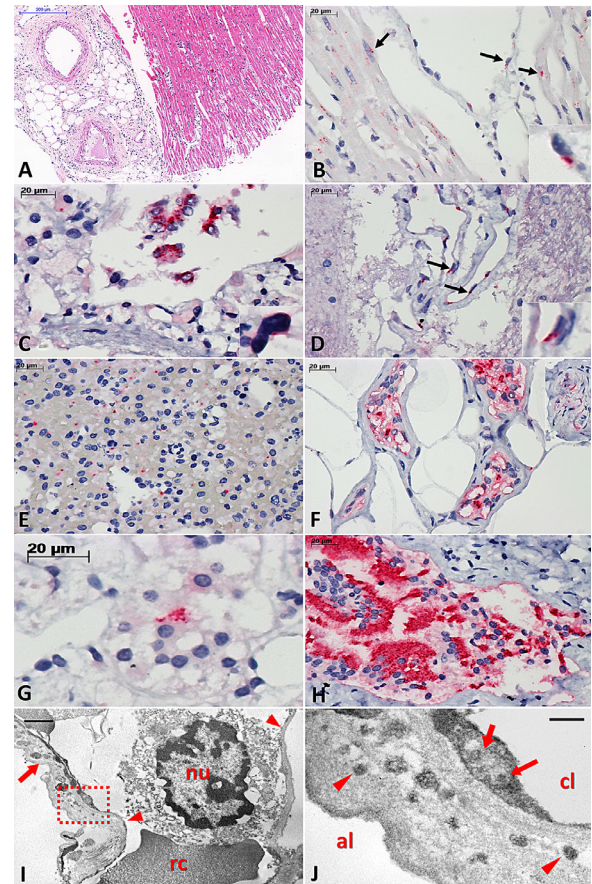
presentation of severe COVID-19 in SARS-CoV-2 infected children with severe comorbidities, especially under the age of one year [6]. A significant increase in aminotransferases and worsening of previous cholestasis was clinically observed in this patient. Histology revealed cholestatic hepatitis, with hepatocyte syncytial changes and the presence of SARS-CoV-2 antigens in hepatocytes. Other viral infections (cytomegalovirus and herpes) were excluded and, therefore, we attributed the hepatic changes in this child to a combination of SARS-CoV-2 infection and haemodynamic alterations.

The other three patients of our series (patients 3 to 5) were previously healthy, fulfilled the WHO/CDC criteria for MIS-C and had distinct clinical courses, with characteristic findings on autopsy [8,9]. They had similar ages (8 to 11 years), were African descendants, and were obese or overweight. Only one patient had other comorbidities (sickle cell trait). Despite having in common high levels of markers of systemic inflammation and progression to shock, the clinical-pathological distinct presentations of these patients indicate a range of possible individual responses to SARS-CoV-2 infection in children with MIS-C: myocarditis, colitis and acute encephalopathy with refractory seizures.
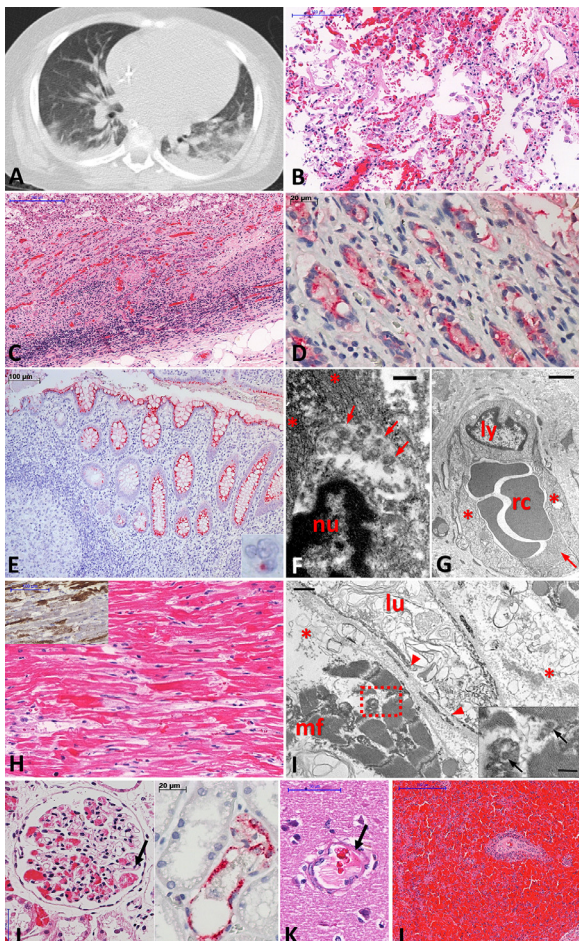
Fig. 4. Pathology of fatal MIS-C related to COVID-19 in patient 4. (A) Chest CT with ground-glass opacities and consolidations, mainly in posterior areas of the left lower lobe. (B) Focal exudative diffuse alveolar damage; H&E. (C-D) Acute colitis (C, H&E) with detection of SARS-CoV-2 N antigen by IHC in the intestinal glands (D). (E) Surgical specimen of coecal appendix showing inflammatory infiltrate in the lamina propria and expansion of Peyer's patch. In red, immunolabelling of SARS-CoV-2 N antigen in the epithelial cells and in some macrophages in the germinative centres (inset). (F) High magnification electron micrograph of a fragment of the intestinal wall showing part of a smooth muscle cell (nu, nucleus) with the typical bundles of cytoplasmic myofilaments (asterisks). Note the presence of several coronavirus particles within the cell (some of them are indicated by arrows). Bar: 200 nm. (G) Ultrastructural aspect of a high endothelial venule in the intestinal wall. Confirming the findings of light microscopy, the image shows a lymphocyte (ly) passing between plump endothelial cells (asterisks). The lumen is filled by red blood cells (rc) and fibrin (arrow). Bar: 2 μm. (H) Contraction band necrosis in the myocardium, with positive detection of C4d by immunohistochemistry (inset). (I) Electron micrograph of myocardium presenting the ultrastructural feature of necrosis with areas devoid of myofibrils (asterisks) in infected cardiomyocytes. An abnormal vessel can be seen, presenting endothelial rupture (arrowheads) and large membrane-bound vacuoles that fill the lumen (lu). The inset shows two viral particles (arrows) near a degenerating myofibril. Bar: 1 μm; Inset bar: 200 nm. (J) Microthrombi in glomerular capillaries and detection of SARS-CoV-2 N antigen by IHC in epithelial ductular cells. (K) Fibrinoid thrombus in a cerebral arteriole (arrow); H&E. (L) Intense lymphoid hypoplasia in the spleen and red pulp haemorrhage; H&E.

Fig. 5. Pathology of fatal MIS-C related to COVID-19 in patient 5 (lung and heart). (A) Chest tomography showing sparse and small areas of ground-glass infiltrate (arrow). (B) Pulmonary thrombus in a medium sized artery; H&E. The inset shows an alveolar cell (cytoplasm in red) with positive expression of SARS-CoV-2 N antigen by IHC. (C) Electron micrograph showing a congested capillary within an alveolar septum. Note the ultrastructural feature of the disruption of the blood−air barrier (arrow) allowing the extravasation of red blood cells (rc) into the alveolar lumen (al). Inset: Several viral particles on the alveolar surface. Bar: 2 μm; Inset Bar: 200 nm. (D) High magnification electron micrograph of an immunolabelled section from the lung (antibody: SARS-CoV-2 anti-N protein, visualized with 10-nm protein A-gold). Several gold particles mark a virus (arrow) in the cytoplasm of a pneumocyte type I (pn); notice the presence of cellular debris in the alveolar lumen (al). Bar: 200 nm. (E) The echocardiography parasternal short axis view shows hyperechogenic left coronary artery, suggesting coronaritis. (F) Cardiac endothelial cell expression of SARS-CoV-2 N antigen by IHC (blue square and inset). (G) High magnification electron micrograph of the myocardium showing a viral particle (arrow) within a membrane-bound vacuole (arrowhead) adjacent to a sarcomeric Z line (Z); mf: ruptured myofilaments. Bar: 200 nm. (H) High magnification electron micrograph of an immunolabelled section from the heart (antibody: SARS-CoV-2 anti-N protein). A virus particle (arrow) labelled with colloidal gold can be seen within the cytoplasm of a cardiomyocyte; spike-like projections (thin arrow) are visible; the arrowheads indicate membranes invaginations of the intercalated disc.

The patients with MIS-C had mild lung injury related to SARS-CoV-2 infection, with a small amount of antigen detected in the distal airways by IHC, without the typical cytopathic changes in pneumocytes seen in adults [16]. Alveolar oedema and vascular thrombi were the main pulmonary findings, which may be due to COVID-19 and/or other associated conditions, such as cardiac failure and bacterial infection [19,21]. These findings indicate that the virus typically infects the respiratory tract, leading to mild disease, as usually described in children, raising questions as to whether children have components of the local pulmonary immune response that can
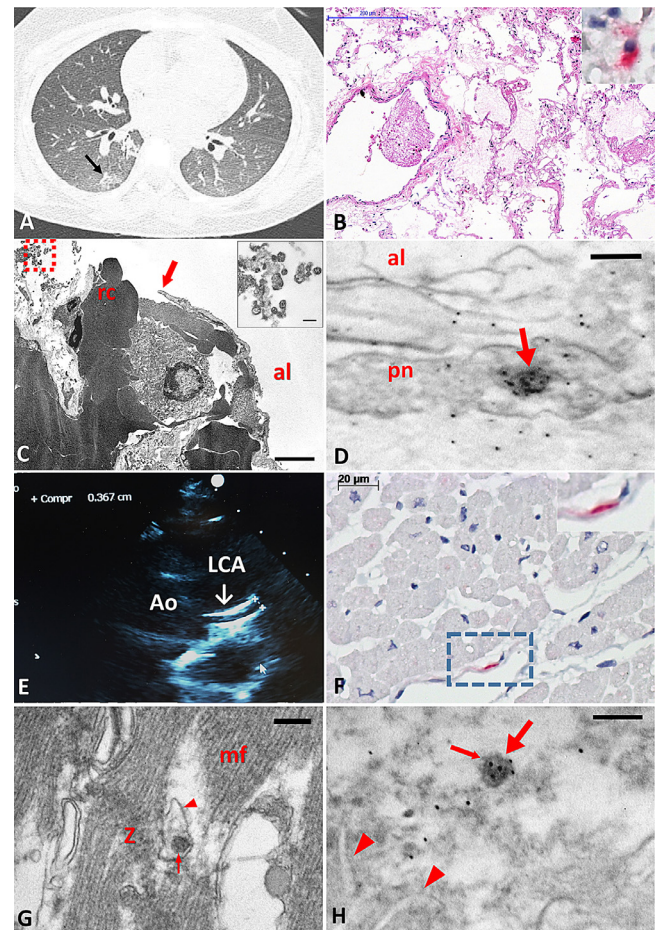
protect them from the virus [22]. Another suggested protective factor from severe respiratory illness in COVID-19 in infants and children is the developmental regulation of TMPRSS2 [23].

After airway infection and systemic spread, SARS-CoV-2 can infect several organs, with variable clinical repercussions. Notably, in the children with MIS-C, we observed viral infection in endothelial cells, mainly in cardiac and brain vessels, as well as in parenchymal cells of various tissues. In patient 3, we observed that SARS-CoV-2 infection in cardiomyocytes and cardiac endothelium induced severe myocarditis, with diffuse perivascular interstitial inflammatory infiltrate and cardiac necrosis, leading to cardiac failure (type I tissue response) [11]. Two other studies reported myocarditis in adolescents with COVID-19 [12,24]. In patient 3, besides the identification of SARS-
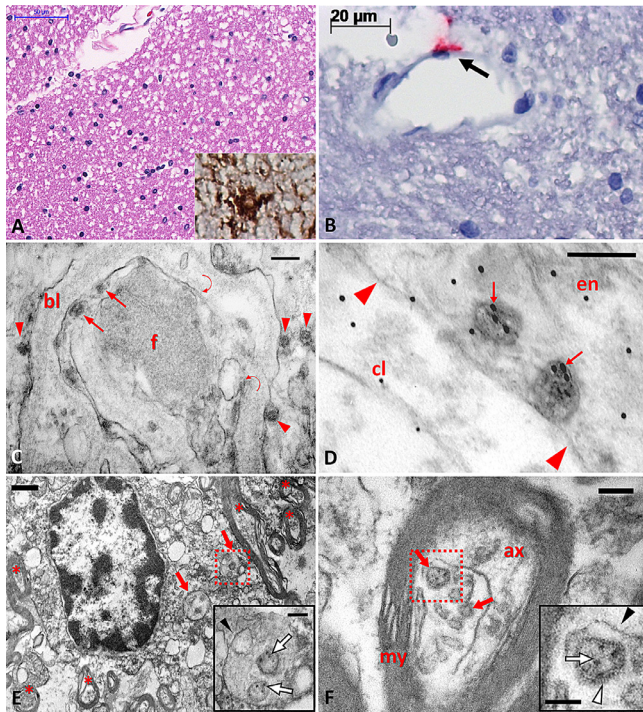
Fig. 6. Pathology of fatal MIS-C related to COVID-19 in patient 5 (brain). (A) Brain with reactive microglia, and perivascular and parenchymal oedema. Inset: GFAP immunodetection showing vacuolar neuropil. (B) Detection of SARS-CoV-2 N antigen by IHC in intracerebral perivascular astrocytes (arrow). (C) High magnification electron micrograph showing a brain capillary whose lumen is filled with fibrin (f). Viral particles are found inside the endothelial cell (arrows) as well as in perivascular astrocytes (arrowheads). Note that the basal lamina (bl) organization is missing where the endothelial cell is ruptured (curved arrows). Bar: 200 nm. (D) High magnification electron micrograph of an immunolabelled section from the brain (antibody: SARS-CoV-2 anti-S2 protein, visualized with 10-nm protein A-gold). Gold particles are highlighted with thin arrows in two virions localized within an endothelial cell (en) of a brain capillary vessel; arrowheads indicate the plasma membrane of the cell facing the capillary lumen (cl). Bar: 200 nm. (E) Electron micrograph showing a cell body of an oligodendrocyte surrounded by myelinated axons (asterisks). Note an extensive disorganization of the cytoplasm with vesiculation, which is typical of coronavirus infection. Some vesicles (arrows) contain virus-like particles. Inset: High magnification of an intracellular vesicle showing its membrane boundary (black arrowhead) and viral particles consistent in size and shape with the Coronaviridae family (white arrows point to nucleocapsids). Bar: 200 nm; Inset bar: 100 nm. (F) Electron micrograph of an axon surrounded by a myelin (my) sheath in the brain. Virus-like particles (arrows) are found inside a vesicle in the axoplasm (axe). Inset: higher magnification of a virus, showing electron dense dots (white arrow) resembling nucleocapsids, and spikes (white arrowhead) projecting from the surface of the viral envelope; the black arrowhead highlights the membrane of the vesicle. Bar: 200 nm; Inset bar: 100 nm. We show for the first time the presence of SARS-CoV-2 in the brain tissue of a child with MIS-C with acute encephalopathy.

CoV-2 in the heart by EM as previously described, IHC detected SARS-CoV-2 antigen in other organs, reinforcing the hypothesis that a direct effect of SARS-CoV-2 on tissues is involved in the pathogenesis of MIS-C [11]. SARS-CoV-2 was also detected by EM in the heart of the two other patients with MIS-C (patients 4 and 5), neither of which had cardiac inflammation, although patient 4 suffered heart tissue necrosis and cardiac dysfunction. Endothelial cell injury in COVID-19 seems to play a critical role in the pathogenesis of the disease, leading to thrombotic events in the pulmonary and systemic circulations, with a wide range of clinical manifestations [21,25,26]. EM demonstrated not only the presence of viral particles in endothelial cells, but also cellular and tissue structural changes, such as disrupted capillary walls associated with fibrin clot formation.

One of our patients with MIS-C (patient 5) had a predominantly neurological clinical manifestation, characterized by status epilepticus, evidenced throughout hospitalization. Although neurological manifestations have been described in patients with COVID-19, with

an increasing number of studies showing their prevalence and spectrum, the occurrence of seizures is rare [1,3−6]. In a series of 27 children with MIS-C, four patients had neurological symptoms, including encephalopathy, headache, brainstem signs with dysarthria or dysphagia, meningism, and cerebellar ataxia. In common, these children presented hypodensity of the splenium of the corpus callosum, possibly representing focal intramyelinic oedema secondary to inflammation [27]. Two possible mechanisms have been proposed for neurological symptoms: an exposure of the immune system to new central nervous system (CNS) antigens as a result of SARS-CoV-2-induced endotheliopathy; and neurological symptoms as part of the systemic autoinflammatory disease [28]. In patient 5, SARS-CoV-2 was identified in the cerebral endothelium and in perivascular astrocytes by IHC, associated with microglial reactivity and cerebral oedema. EM evidenced viral particles in the brain endothelial cells and in glial cells, and disorganization of the blood-brain barrier. This is the first study that reports the presence of SARS-CoV-2 in the brain tissue of a child with MIS-C with acute encephalopathy. Our findings are in line with the hypothesis that SARS-CoV-2 crosses the blood-brain barrier leading to an immune-directed attack on the CNS [27,28]. However, we cannot rule out that the refractory seizures presented by our patient and the cellular changes observed in the brain may also have resulted from other mechanisms, such as hypoxia and toxic-metabolic alterations, in addition to the probable virus-induced injury. This patient had negative SARS-CoV-2 RT-PCR test, and the clinical diagnosis of COVID-19 was presumptive. Serology was not performed during hospitalization, and a post-mortem serology on a stored blood sample was negative. Interestingly, SARS-CoV-2 infection was only confirmed by the finding of viral particles by EM and positive IHC in tissues. It is notable that the EM and IHC show the presence of the virus more than 20 days after the onset of symptoms. This case shows that MIS-C can occur even without a history of positive RT-PCR, and physicians should be aware of these possible atypical presentations [29,30].

MIS-C involves gastrointestinal (GI) symptoms in the majority of patients, including abdominal pain, vomiting and diarrhoea [31]. The analysis of patient 4 brings important information about the GI involvement in MIS-C, leading to nonspecific pain, diarrhoea, and acute abdomen, and including the possibility of excretion of virions in the faeces. In this case, we observed diffuse colon inflammation, with inflammatory infiltration in glands and intense immunostaining for SARS-CoV-2, in addition to viral particles identified by EM. This is the first study that reports the presence of SARS-CoV-2 in the intestinal tissue of a child with MIS-C with acute colitis. As the intestinal epithelium has a large number of ACE2 receptors, this suggests an intestinal intraluminal route of infection, through the swallowing of contaminated respiratory secretions, leading to colitis, as occurs with enteroviruses [32,33]. The ultrastructural analysis of intestinal tissue showed SARS-CoV-2 particles within the smooth muscle layer and in endothelial cells; we suggest that inflammation, smooth muscle damage and microthrombotic/ischaemic events are likely responsible for the frequent GI symptoms observed in patients with MIS-C. Histology from an ileocolic resection in a patient with MIS-C has recently shown a spectrum of findings that includes lymphocytic inflammation, venous microthrombi, arteritis, and necrotizing lymphadenitis [31].

In addition to the findings in specific target organs, our patients with MIS-C had several other alterations likely related to the systemic inflammation and shock, such as acute tubular necrosis and glomerular microthrombi in the kidneys, and centrilobular necrosis in the liver [34,35]. The finding of haemophagocytosis, splenitis, lymphoid hypoplasia, and SARS-CoV-2 antigens in mononuclear cells indicate a direct association of the virus with severe COVID-19 immune dysfunction. The three patients were obese or overweight. Obesity in children and adolescents is a risk factor associated with a higher number of SARS-CoV-2 infections, development of COVID-19

pneumonia, and hospitalization [36,37,38]. Obesity is also considered a risk factor for MIS-C. In a systematic review of MIS-C with 662 patients, 50.8% of the children were overweight or obese [37]. The authors summarized the possible mechanisms involved in the association of obesity and MIS-C: accumulation of inflammatory cells in the adipose tissue, proinflammatory fat tissue cytokines, impaired respiratory function, and high levels of SARS-CoV-2 binding receptors in adipose cells [37]. Using IHC, Schurink et al. found SARS-CoV-2 N-protein in the fat tissue in 9−18% of adult patients with fatal COVID-19 [38]. Interestingly, in our patients SARS-CoV-2 antigens were present in fat tissue of the hypodermis, meso-, and epicardium of patients 1 to 4 (Table 3, appendix p.4 and p.5).

Our study has some limitations; a) it is a descriptive analysis of a small number of patients, which limits the pathological conclusions and the generalisability of the findings to the general population. However, and fortunately, SARS-CoV-2 causes mainly mild disease in children, both in Brazil and in other countries, with few autopsies being reported so far. The cases presented here are in line with the previous larger clinical series of severe COVID-19/MIS-C that report a potentially severe systemic inflammatory syndrome, with preferential involvement of non-pulmonary organs, such as the heart and GI tract [11,12,20,29−31,39,40]; b) there was no systematic testing for SARS-CoV-2 infection in all patients (serology and RT-PCR) during hospitalization, which made the diagnosis confirmation more difficult; c) the autopsy was performed with a minimally-invasive method, which can limit pathological interpretation, such as with the brain findings, where the alterations can be sparse and focal [28]. However, for the families, MIA is a more acceptable post-mortem

examination method for the paediatric population; d) the overlap of bacterial sepsis in patient 5 can alter the data interpretation; however, bacterial infection in this patient was acquired after ten days of hospitalization and did not have any influence on the MIS-C clinical presentation on admission; e) Patient 5 did not have a confirmed diagnosis of COVID-19 before autopsy. Although there was no report of direct contact with a person with proven COVID-19, this patient came from an area with a high incidence of COVID-19 cases, during the pandemic peak period. Although the post-mortem diagnosis of COVID-19 is commonly reported in adults, the MIS-C CDC and WHO criteria do not include a pathologic criterion (from autopsy or biopsy samples) [8,9]. Our results indicate the possibility of COVID-19/MIS-C even with negative swab RT-PCR and serology, as was previously reported [30]. f) post-mortem autolysis may have limited the performance of IHC, RT-PCR and EM; g) EM findings may show some artefacts related to samples obtained from paraffin blocks; however, tissue retrieval from paraffin blocks allowed us to focus on areas with histological alterations and positive immunostaining for SARS-CoV-2.

As seen in our case series, COVID-19 can be severe in children, including fatal events. We showed that SARS-CoV-2 has great invasive potential and can infect various cell and tissue types, and the target organ for the predominant clinical manifestation varies amongst individuals. Our findings indicate two major patterns of severe COVID-19 in children and adolescents: a primarily pulmonary manifestation of the disease, with SARS-CoV-2 pneumonia, respiratory failure, need for ventilatory support and diffuse alveolar damage by histology (corresponding to SARS), or a multisystem inflammatory syndrome with the involvement of several organs and tissues (Fig. 7).
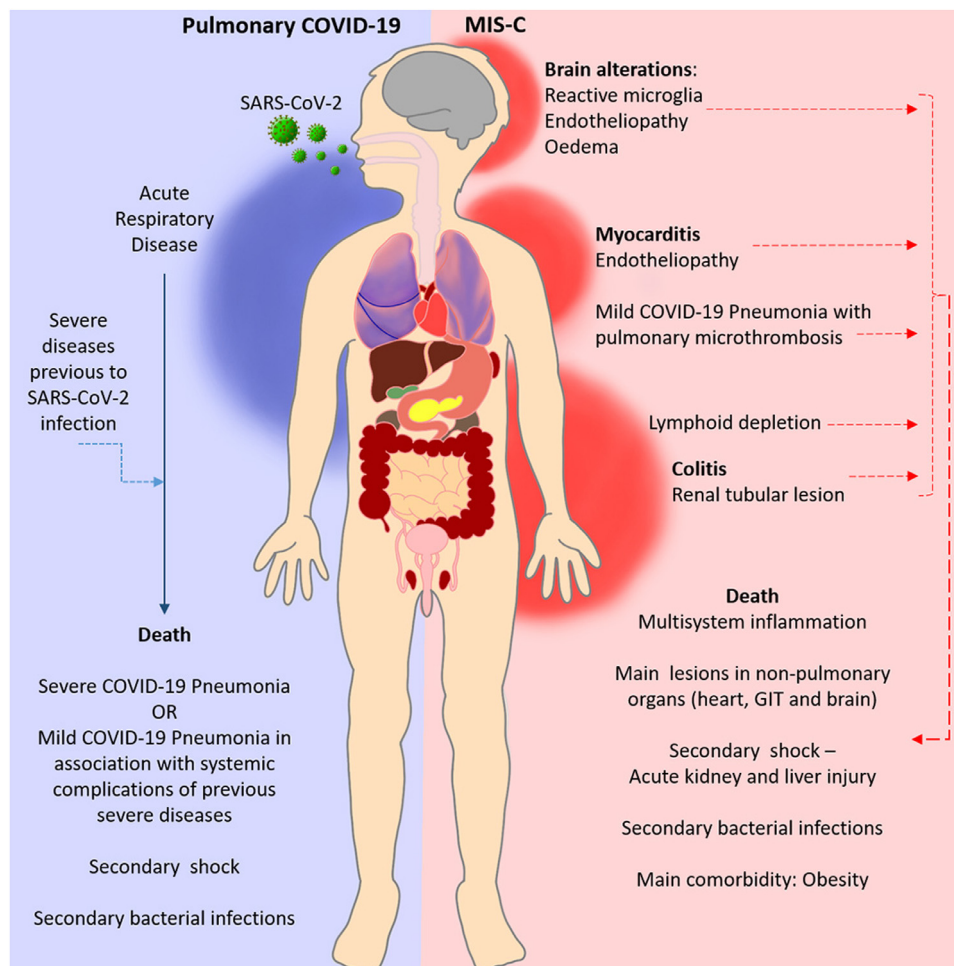

Fig. 7. Summary of pathological findings in five paediatric patients who died with COVID-19.

Children with major comorbidities (in our series, one adolescent with a terminal neoplastic disease and a child with a complex genetic disorder) seem to preferentially present the pulmonary form of the disease. Patients with MIS-C, despite having many factors in common, may have several forms of clinical-pathological presentation, possibly representative of different disease phenotypes. Cardiac dysfunction associated with high levels of markers of cardiac injury and myocardial necrosis seems to be prevalent in patients with severe MIS-C (two in three patients in this series), as has been reported in clinical studies [39,40]. Abdominal pain, a frequent symptom in MIS-C, is likely related to SARS-CoV-2-induced intestinal inflammation, and can be the predominant manifestation. Despite the clinical-pathological spectrum of the disease, EM showed that damage to the pulmonary epithelial lining, myocardial damage with sarcomere rupture, and endothelial injury associated with tiny fibrin clots are common characteristics in these patients. The mechanisms involved in tissue damage may include direct viral effect and/or host systemic immune response. The presence of SARS-CoV-2 antigens and virions in trophic and endothelial cells in different organs, associated with ultrastructural changes in these cells, reinforces the hypothesis that a direct effect of SARS-CoV-2 on tissues is involved in the pathogenesis of MIS-C. The individual factors related to each form of severe COVID-19 presentation in children and adolescents still need to be determined.

Funding

Data sharing

All data used and obtained in this study are available in the manuscript and supporting information.

Contributors

JFF, AMCV, FAR, DMF, MABCG, WBC, GNL, AFD and MCS were involved in the care of the patients. ANDN, RAAM, TM, LFFS, PHNS and MD collected and interpreted the autopsy data. MSGG, CTK and JRRP performed and interpreted the molecular data. EGC performed and interpreted the EM analysis. ANDN, EGC and MD prepared the original draft of the manuscript. All authors reviewed and approved the final version of the manuscript.

Ethics committee approval

This work was approved by the HC-FMUSP Ethical Committee (protocol no. 3951.904).

Declaration of Competing Interest

We declare no competing interests.

Acknowledgements

Supplementary materials

Supplementary material associated with this article can be found in the online version at doi:10.1016/j.eclinm.2021.100850.

References

[1] Götzinger F, Santiago-García B, Noguera-Julián A, et al. COVID-19 in children and adolescents in Europe: a multinational, multicentre cohort study. Lancet Child Adolesc Health 2020;4(9):653–61. doi: 10.1016/S2352-4642(20)30177-2.

[2] Wu Z, McGoogan JM. Characteristics of and important lessons from the coronavirus disease 2019 (COVID-19) outbreak in China: summary of a report of 72 314 cases from the Chinese center for disease control and prevention. JAMA 2020;323 (13):1239–42. doi: 10.1001/jama.2020.2648.

[3] Stokes EK, Zambrano LD, Anderson KN, et al. Coronavirus disease 2019 case surveillance - United States, January 22-May 30, 2020. MMWR Morb Mortal Wkly Rep 2020;69(24):759–65 Published 2020 Jun 19. doi: 10.15585/mmwr.mm6924e2.

[4] Bixler D, Miller AD, Mattison CP, et al. SARS-CoV-2-associated deaths among persons aged <21 Years - United States, February 12-July 31, 2020. MMWR Morb Mortal Wkly Rep 2020;69(37):1324–9 Published 2020 Sep 18. doi: 10.15585/mmwr.mm6937e4.

[5] Zachariah P, Johnson CL, Halabi KC, et al. Epidemiology, clinical features, and disease severity in patients with coronavirus disease 2019 (COVID-19) in a children's hospital in New York City, New York. JAMA Pediatr 2020;174(10):e202430. doi: 10.1001/jamapediatrics.2020.2430.

[6] Liguoro I, Pilotto C, Bonanni M, Ferrari ME, Pusiol A, Nocerino A, Vidal E, Cogo P. SARS-COV-2 infection in children and newborns: a systematic review. Eur J Pediatr 2020;179(7):1029–46 Jul. doi: 10.1007/s00431-020-03684-7.

[7] Ministério da Saúde-Secretaria de Vigilância em Saúde. Boletim Epidemiológico Especial— Semana Epidemiológica 44 (27/12/2020 a 2/1/2021). Available at: https://www.gov.br/saude/pt-br/media/pdf/2021/janeiro/07/boletim_epidemiologico_covid_44.pdf Accessed on 12 February 2021.

[8] Centers for Disease Control and Prevention Health Alert Network (HAN). Multisystem inflammatory syndrome in children (MIS-C) associated with coronavirus disease 2019 (COVID-19). Available at: https://emergency.cdc.gov/han/2020/han00432.asp . Accessed on October 28, 2020.

[9] World Health Organization. Multisystem inflammatory syndrome in children and adolescents with COVID-19: scientific Brief. 2020. Available at: https://www.who.int/publications-detail/multisystem-inflammatory-syndrome-in-children-and-adolescents-with-covid-19 . Accessed on October 28, 2020.

[10] Levin M. Childhood multisystem inflammatory syndrome - a new challenge in the pandemic. N Engl J Med 2020;383(4):393–5 Jul 23. doi: 10.1056/NEJMe2023158.

[11] Dolhnikoff M, Ferreira Ferranti J, de Almeida Monteiro RA, et al. SARS-CoV-2 in cardiac tissue of a child with COVID-19-related multisystem inflammatory syndrome [published correction appears in lancet child adolesc health. 2020 Oct;4 (10):e39]. Lancet Child Adolesc Health 2020;4(10):790–4. doi: 10.1016/S2352-4642(20)30257-1.

[12] Craver R, Huber S, Sandomirsky M, McKenna D, Schieffelin J, Finger L. Fatal eosinophilic myocarditis in a healthy 17-year-old male with severe acute respiratory syndrome coronavirus 2 (SARS-CoV-2c). Fetal Pediatr Pathol 2020;39(3):263–8 Jun. doi: 10.1080/15513815.2020.1761491.

[13] Baud D, Greub G, Favre G, et al. Second-trimester miscarriage in a pregnant woman with SARS-CoV-2 infection. JAMA 2020;323(21):2198–200. doi: 10.1001/jama.2020.7233.

[14] Lopez L, Colan SD, Frommelt PC, et al. Recommendations for quantification methods during the performance of a pediatric echocardiogram: a report from the pediatric measurements writing group of the American society of echocardiography pediatric and congenital heart disease council. J Am Soc Echocardiogr 2010;23(5):465–577. doi: 10.1016/j.echo.2010.03.019.

[15] McCrindle BW, Rowley AH, Newburger JW, et al. Diagnosis, treatment, and long-term management of Kawasaki disease: a scientific statement for health professionals from the American heart association [published correction appears in circulation. 2019 Jul 30;140(5):e181-e184]. Circulation 2017;135(17):e927–99. doi: 10.1161/CIR.0000000000000484.

[16] Nunes Duarte-Neto A, de Almeida Monteiro RA, da Silva LFF, et al. Pulmonary and systemic involvement of COVID-19 assessed by ultrasound-guided minimally invasive autopsy [published online ahead of print, 2020 May 22]. Histopathology 2020. doi: 10.1111/his.14160.

[17] Centers for Disease Control and Prevention—Coronavirus Disease 2019 (COVID-19). Interim guidelines for collecting, handling, and testing clinical specimens

from persons for coronavirus disease 2019 (COVID-19). Available at: https://www.cdc.gov/coronavirus/2019-ncov/lab/guidelines-clinical-specimens.html (accessed 25 February 2021).

[18] Corman VM, Landt O, Kaiser M, et al. Detection of 2019 novel coronavirus (2019-nCoV) by real-time RT-PCR. Euro Surveill 2020;25:2000045.

[19] Levi M, van der Poll T. Coagulation and sepsis. Thromb Res 2017;149:38–44. doi: 10.1016/j.thromres.2016.11.007.

[20] Rimensberger PC, Kneyber MCJ, Deep A, et al. Caring for critically ill children with suspected or proven coronavirus disease 2019 infection: recommendations by the scientific sections' collaborative of the european society of pediatric and neonatal intensive care. Pediatr Crit Care Med 2021;22(1):56–67. doi: 10.1097/PCC.0000000000002599.

[21] Dolhnikoff M, Duarte-Neto AN, de Almeida Monteiro RA, et al. Pathological evidence of pulmonary thrombotic phenomena in severe COVID-19. J Thromb Haemost 2020;18(6):1517–9. doi: 10.1111/jth.14844.

[22] Dhochak N, Singhal T, Kabra SK, Lodha R. Pathophysiology of COVID-19: why children fare better than adults? Indian J Pediatr 2020;87(7):537–46. doi: 10.1007/s12098-020-03322-y.

[23] Schuler BA, Habermann AC, Plosa EJ, et al. Age-determined expression of priming protease TMPRSS2 and localization of SARS-CoV-2 in lung epithelium. J Clin Invest 2021;131(1):e140766. doi: 10.1172/JCI140766.

[24] Gnecchi M, Moretti F, Bassi EM, et al. Myocarditis in a 16-year-old boy positive for SARS-CoV-2. Lancet 2020;395(10242):e116. doi: 10.1016/S0140-6736(20)31307-6.

[25] Varga Z, Flammer AJ, Steiger P, et al. Endothelial cell infection and endotheliitis in COVID-19. Lancet 2020;395(10234):1417–8. doi: 10.1016/S0140-6736(20)30937-5.

[26] Goshua G, Pine AB, Meizlish ML, et al. Endotheliopathy in COVID-19-associated coagulopathy: evidence from a single-centre, cross-sectional study. Lancet Haematol 2020;7(8):e575–82. doi: 10.1016/S2352-3026(20)30216-7.

[27] Abdel-Mannan O, Eyre M, Löbel U, et al. Neurologic and radiographic findings associated With COVID-19 infection in children [published online ahead of print, 2020 Jul 1]. JAMA Neurol 2020:e202687. doi: 10.1001/jamaneurol.2020.2687.

[28] Matschke J, Lütgehetmann M, Hagel C, et al. Neuropathology of patients with COVID-19 in Germany: a post-mortem case series [published online ahead of print, 2020 Oct 5]. Lancet Neurol 2020;19(11):919–29. doi: 10.1016/S1474-4422(20)30308-2.

[29] Dufort EM, Koumans EH, Chow EJ, et al. Multisystem inflammatory syndrome in children in New York state. N Engl J Med 2020;383(4):347–58. doi: 10.1056/NEJMoa2021756.

[30] Feldstein LR, Rose EB, Horwitz SM, et al. Multisystem inflammatory syndrome in U.S. children and adolescents. N Engl J Med 2020;383(4):334–46. doi: 10.1056/NEJMoa2021680.

[31] Sahn B, Eze OP, Edelman MC, Chougar CE, Thomas RM, Schleien CL, Weinstein T. Features of intestinal disease associated with COVID-related multisystem inflammatory syndrome in children. J Pediatr Gastroenterol Nutr 2020 Sep 22. doi: 10.1097/MPG.0000000000002953.

[32] Hamming I, Timens W, Bulthuis ML, Lely AT, Navis G, van Goor H. Tissue distribution of ACE2 protein, the functional receptor for SARS coronavirus. A first step in understanding SARS pathogenesis. J Pathol 2004;203(2):631–7. doi: 10.1002/path.1570.

[33] Chan KH, Sridhar S, Zhang RR, et al. Factors affecting stability and infectivity of SARS-CoV-2. J Hosp Infect 2020;106(2):226–31. doi: 10.1016/j.jhin.2020.07.009.

[34] Su H, Yang M, Wan C, et al. Renal histopathological analysis of 26 postmortem findings of patients with COVID-19 in China. Kidney Int 2020;98(1):219–27. doi: 10.1016/j.kint.2020.04.003.

[35] Sonzogni A, Previtali G, Seghezzi M, et al. Liver histopathology in severe COVID 19 respiratory failure is suggestive of vascular alterations. Liver Int 2020;40(9):2110–6. doi: 10.1111/liv.14601.

[36] Leon-Abarca JA. Obesity and immunodeficiencies are the main pre-existing conditions associated with mild to moderate COVID-19 in children [published online ahead of print, 2020 Aug 12]. Pediatr Obes 2020:e12713. doi: 10.1111/ijpo.12713.

[37] Ahmed M, Advani S, Moreira A, et al. Multisystem inflammatory syndrome in children: a systematic review. EClinicalMedicine 2020;26:100527. doi: 10.1016/j.eclinm.2020.100527.

[38] Schurink B, Roos E, Radonic T, et al. Viral presence and immunopathology in patients with lethal COVID-19: a prospective autopsy cohort study. Lancet Microbe 2020;1(7):e290–9. doi: 10.1016/S2666-5247(20)30144-0.

[39] Grimaud M, Starck J, Levy M, et al. Acute myocarditis and multisystem inflammatory emerging disease following SARS-CoV-2 infection in critically ill children. Ann Intensive Care 2020;10:69.

[40] Belhadjer Z, Méot M, Bajolle F, et al. Acute heart failure in multisystem inflammatory syndrome in children (MIS-C) in the context of global SARS-CoV-2 pandemic. Circulation 2020 10.1161/CIRCULATIONAHA.120.048360.